A Lower Size, Weight Acquisition and Tracking System for Airborne Quantum Communication

Chengxiang Tu, Jiayi Shen, Jiansheng Dai, Liang Zhang, and Jianyu Wang

***Abstract*—The features of unmanned aerial vehicles (UAVs), such as strong manoeuvrability, small size, and light weight, make them considered to participate in free space optical (FSO) quantum communication, becoming an important part of the Space-Air-Ground Integrated Network. However, research reports on small-sized drones based long-range optical quantum link are few. A major challenge is that traditional opto-mechanical structure is difficult to adapt to small UAV platforms. Here, a lower size, weight, and power (SWaP) acquisition and tracking system prototype is developed, and its greatest advantage is that the system can be easily integrated into small flying platforms and quickly build a long-distance quantum communication link. The prototype weighs less than 8 kg. A small-sized two-axis mirror mechanism is designed for wide-range acquisition and tracking. Moreover, the system can automatically point to ground station. The SWaP acquisition and tracking system can support quantum key distribution (QKD) link and general FSO link by drones. In the 7 km air-to-ground demonstration, the acquisition and tracking system prototype is tested in practice, which is suspended under the small six-rotor UAV platform, and a special passive vibration isolation unit is added in between. A ten-minute continuous and stable beacon tracking proves that the system can quickly and automatically align.**

***Index Terms*—Electro-optical system, free-space link, drone, quantum network.**

I. Introduction

QUANTUM communication is a new type of communication mode developed in recent years that stems from the need to keep both parties confidential, especially in the military. With the rapid development of the internet industry, increasing attention has been given to the information security of users and enterprises, so quantum communication has broad application prospects [1], [2]. At present, quantum secure communication has been successfully applied to optical fibre communication [3], [4] and satellite optical communication [5], [6]. Several works on drone-based quantum networks have been published [7], [8], [9].

UAV technology has developed rapidly in recent years. Its advantages, such as strong manoeuvrability, small size, and light weight, make UAVs considered to participate in FSO quantum communication, becoming an important part of the Space-Air-Ground Integrated Network. The UAV can act as the relay point, which can better reflect the advantages of the FSO. For instance, the quantum satellite Micius is a low-orbit satellite, and the visible time to the ground station is less than 10 minutes [5]. If UAVs act as relay points at middle and low altitudes, the visible time between the satellite and the UAV can be extended. This can also overcome the challenges of bad weather on the communication link: when the UAV is at 5 km, it is above most of the clouds. Demonstrations of optical links between aircraft and satellites have long been reported [10], which shows the feasibility of the above case. Therefore, UAVs can be covered on the scale of space and time as needed and interconnected with satellites and ground optical fibres, and finally, a global quantum communication network can be constructed. Moreover, UAVs can also be used as relay points for land–sea networks, and network integration will extend to deep-sea communications. There have been many works on the research and application of atmosphere-ocean optical communication systems [11], [12], [13]. Reference [14] proposed that a communi-cation link can be built among the ground station, UAV and high-speed train: passenger mobile data are transferred to the base station through the UAV relay, so the passengers can surf the internet through WIFI in the train. In the remote sensing field, due to the growth in scale and resolution of airborne/aerial scanning data [15], the captured data can be transmitted to the ground station through laser communication. In the future, UAVs will be used as communication terminals or relays in the form of clusters. Fig. 1 is a schematic diagram of the envisaged optical quantum communication network [16], [17].

Although airborne communication has broad application prospects, its demonstrations are rare. Aircraft feature a large uncertain area, fast motion, and strong vibration. Therefore, a key problem is that traditional acquisition, tracking and pointing

Manuscript received 30 September 2022; accepted 2 October 2022. Date of publication 10 October 2022; date of current version 19 October 2022. This work was supported in part by the Key Technologies Research and Development Program under Grant 2020YFB2205900, in part by the Youth Innovation Promotion Association of the Chinese Academy of Sciences, and in part by the Shanghai Municipal Science and Technology Major Project under Grant 2019SHZDZX01. *(Corresponding authors: Liang Zhang; Jianyu Wang.)*

Chengxiang Tu is with the Key Laboratory of Space Active Opto-Electronics Technology, Shanghai Institute of Technical Physics, Chinese Academy of Sciences, Shanghai 200083, China, and also with the School of Information Science and Technology, ShanghaiTech University, Shanghai 201210, China (e-mail: tuchx@shanghaitech.edu.cn).

Jiayi Shen and Jiansheng Dai are with the Key Laboratory of Space Active Opto-Electronics Technology, Shanghai Institute of Technical Physics, Chinese Academy of Sciences, Shanghai 200083, China (e-mail: edward2340@163.com; daijiansheng@mail.sitp.ac.cn).

Liang Zhang is with the Key Laboratory of Space Active Opto-Electronics Technology, Shanghai Institute of Technical Physics, Chinese Academy of Sciences, Shanghai 200083, China, and also with the University of Chinese Academy of Sciences, Beijing 100049, China (e-mail: zhliang@mail.sitp.ac.cn).

Jianyu Wang is with the Key Laboratory of Space Active Opto-Electronics Technology, Shanghai Institute of Technical Physics, Chinese Academy of Sciences, Shanghai 200083, China, also with the University of Chinese Academy of Sciences, Beijing 100049, China, and also with the Shanghai Quantum Science Research Center, Shanghai 201315, China (e-mail: jywang@mail.sitp.ac.cn).

Digital Object Identifier 10.1109/JPHOT.2022.3212590

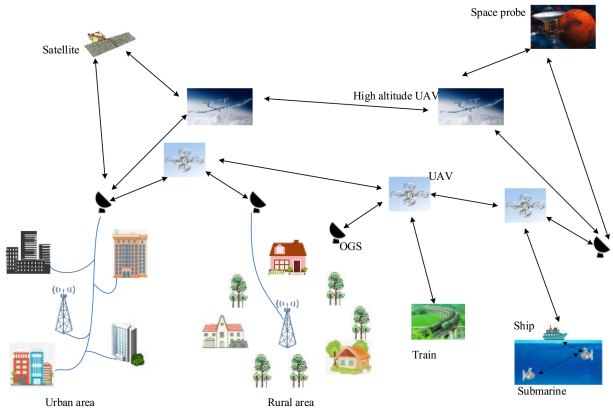

Fig. 1. Future optical quantum communication network.

(ATP) systems are difficult to adapt to aircraft platforms, especially to small UAVs. For large aircraft platform, tracking beacons with two-axis turntable applied in satellite FSO communication is considered to be transferred to airborne communication. Demonstrations of airborne communications have been reported early. In the 1980 s, the United States used two manned airborne platforms (KC-135A aircraft) to launch an air-to-air laser communication demonstration with a maximum distance of 160 km [18]. For its pointing and tracking systems, a major disadvantage was that initial signal acquisition has to be performed manually. Then, in the 1990 s, air-to-air laser communication up to 500 km was achieved on two T-39 aircraft [18], [19]. Its optical subsystem adopted turret mechanical design, the initial pointing was implemented by the radio frequency link to exchange the position status of both terminals, tracking control used coarse-to-fine two-level tracking. In addition, the Europe had demonstrations about aircraft-to-satellite laser communication [20], [21]. In the past decade, airborne laser communication has made little progress. Changchun University of Science and Technology gave a high-speed and long-distance (up to 144 km) laser communication demonstration between two fixed-wing aircraft (Y12) using two-level tracking, with an average acquisition time of 20 s in 2013 [22]. In the same year, Deutsches Zentrum für Luft- und Raumfahrt (DLR) demonstrated air-to-ground laser communication with a maximum link distance of 80 km and an accuracy of up to 20 μrad on the panavia tornado platform [23]. It is noteworthy that the above demonstration platforms are all large aircraft, and the ATP system adopts compound axis control with two-level tracking, which is bulky and heavy. However, small UAVs have stricter restrictions on the system prototype in volume, weight and energy consumption. In 2019, Nanjing University used an eight-rotor UAV distributing quantum keys to two ground stations to achieve quantum communication, with an error of approximately 1 μm in the 100-metre tracking test [7]. But the 100-metre demonstration serve no useful purpose, and beam aperture (only 26.4 mm) does not support longer-range acquisition. So far, research on small-sized drones based long-range optical quantum link is not reported. A major challenge is that the optomechanical structure and ATP system need improvement and innovation. Utilizing larger aircrafts as the carrier platform is unfavourable for the development towards a commercial product. Therefore, it is necessary to designs an ATP system based on small-sized UAV that can build long-range quantum communication links, which will be a significant step in airborne communication.

In this work, a SWaP acquisition and tracking system prototype is developed for the small platforms, and its greatest advantage is that the system can be easily integrated into small flying platforms and can quickly build long-distance quantum communication links. The system adopts the coaxial structure of the transceiver, and the whole prototype weighs less than 8 kg. Based on the traditional tracking system, it is simplified and improved to have the characteristics of a large field of view (FOV) and fast response to complete long-distance rapid acquisition and stable tracking. Moreover, a lightweight passive isolation unit is introduced into the prototype to isolate the platform vibration. In the 7 km drone-to-ground demonstration, the acquisition and tracking system prototype is tested in practice, which is suspended under the small six-rotor UAV platform, showing continuous and stable ATP capabilities. The SWaP acquisition and tracking system can not only support QKD link by drones, but it also supports general FSO link. This research provides an approach to the design of small ATP systems and can serve airborne optical quantum deployment in real environments.

II. System Composition

The UAV platform brings severe vibration spectrum, much higher base motion disturbances, and more restrictive mechanical integration constraints. Here, the system is designed in view of miniaturization, increased agility, robustness and easy integration. The system adopts the coaxial structure of the transceiver. The two-axis mirror, the tracking mechanism adopted by the system, is a fast and wide-range electromechanical actuator used to compensate middle- and low-frequency vibrations, and it only weighs approximately 1.5 kg. The corresponding tracking system is simplified and has the characteristics of strong robustness, fast response and large FOV. With the support of add-on integration module MEMS-IMU (inertial measurement unit), the system can automatically point to ground station. Furthermore, the wire rope isolator (WRI), a passive isolation structure, is used to isolate the prototype from the drone vibrations, especially for high-frequency vibrations. The amplitude frequency curve of WRI rises first and then falls, and the peak value is the resonance frequency. According to the bandwidth of the system, choosing the proper WRI can make the total disturbance suppression bandwidth higher. It weighs less than 100 g meeting the lightweight requirements. The WRI is bolted between the prototype and the platform, which is convenient for disassembly and assembly. All These allow continuous and stable ATP capabilities for prototype with a total weight of less than 8 kg. More details will be described in this article later.

The opto-mechanical block diagram is shown in Fig. 2(a). The acquisition and tracking system is composed of a control board, motor drive module, circular grating module, tracking camera, laser transmitter module and MEMS-IMU. The two-axis mirror

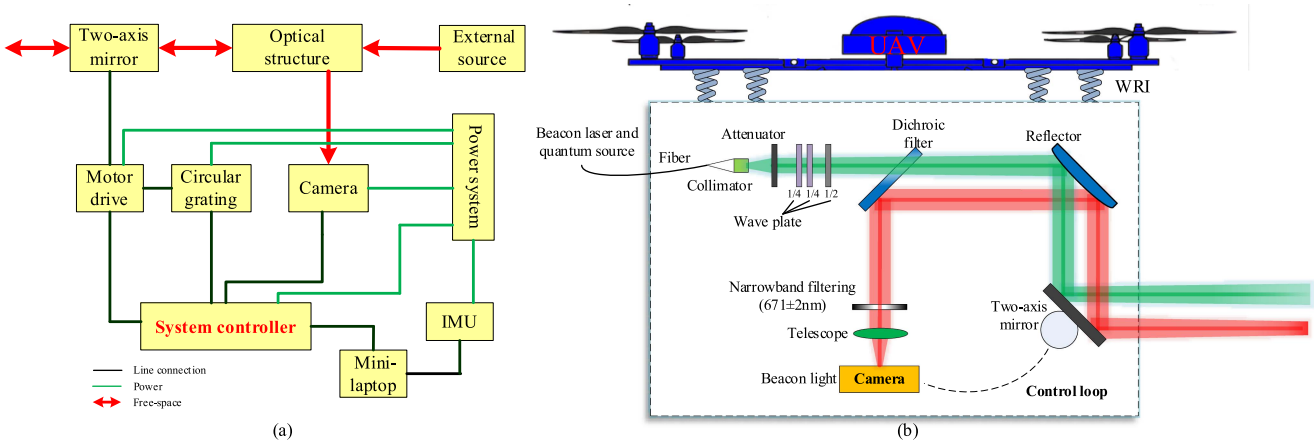

Fig. 2. (a) Acquisition and tracking system block diagram. The electrical signal lines are shown in black and optical signals are in red. The power lines are depicted in green. (b) System optical path. The transceiver coaxial structure is adopted. The 671 nm beacon from the ground station is reflected into the camera system through the two-axis mirror, reflector, and dichroic filter. Narrow-band filtering is adopted to suppress the strong background noise in the urban environment. After passing through the filtering, the beacon is focused into a spot on the CMOS through the telescope. For the communication terminal, a fiber is connected to the source of the external communication system, and the other end is connected to the internal collimator. The source contains beacon and signal (including quantum key distribution) to the ground station. The beacon and quantum signal pass through the same optical fiber and the same optical path. The laser source is directed to the ground station through the attenuator, two quarter-wave plates, half-wave plate, and two reflections.

TABLE I
PERFORMANCE OF THE ACQUISITION AND TRACKING SYSTEM

Parameter		Value
Two-axis mirror	Motor type	Permanent magnet synchronous motor
	Circular grating resolution	0.3 arcsec
	Travel range	Azimuth:±90° Elevation: ±20°
	Pointing accuracy	≤ 0.25°
	Tracking speed	≥ 5°/s
	Bandwidth	> 20 Hz
Tracking camera	Type	CMOS
	FOV	20 mrad ∗ 20 mrad
	Size & frame rate	512 × 512 pixels & 200 Hz
	Beam aperture	50 mm
Beacon laser	Power	10 mW
	Wavelength	815 nm
	Divergence	420 μrad

is driven by the rotary motors, the circular grating returns the motor angle information, the camera detects the spot and returns the spot position information, the laser emits beacon light to the ground terminal, and the MEMS-IMU returns the UAV attitude and position information in Global Navigation Satellite System (GNSS). All the information is sent to the control board, and the whole system is powered by lithium batteries. Additionally, an extra mini-laptop can obtain the real-time data of the system for analysis and debugging. More parameters are shown in Table I.

The system mainly completes the acquisition and tracking of the beacon light. The optical path and structure of the system are shown in Fig. 2(b). In the acquisition stage, an initial set of pointing angles for the acquisition phase is created based on information about the UAV position and attitude supplied by the IMU, and then the controller drives the two-axis mirror to point to the ground station. If the beacon is detected by the camera, the system enters the tracking mode. Ideally, the beacon light spot from the ground station can fall in the centre of the camera. However, due to the movement and vibration of the UAV, atmospheric turbulence and other reasons, the errors always exist. Then, the controller computes the deviation of the spot from the centroid and drives the two-axis mirror to compensate it. The closed-loop control continues running until the spot is lost, and the system will restart acquisition mode. When tracking errors are at a low level, the quantum communication link between the UAV and ground station has been built.

III. TRACKING SYSTEM

The tracking system is used to maintain the communication link against disturbance. As the actuator, the two-axis mirror is composed of two small permanent magnet synchronous motors (PMSMs) and a mirror (Fig. 3), featuring small inertia and fast acting. It can overcome severe vibration and strong manoeuvrability of the airborne platform, to achieve wide-range tracking and fast response. The motor system model can be approximated as a second-order damping system:

$$G\ (s) = \frac{\omega_n^2}{s^2 + 2\xi\omega_n s + \omega_n^2} \tag{1}$$

where ξ is the damping ratio and ω_n is the undamped natural frequency.

The tracking system is a position servo system and should have a fast response while avoiding overshoot to meet the dynamic performance. The motor selected features a slightly small inertia moment, and the motor speed changes frequently when the system is working. As a result, the traditional three-loop

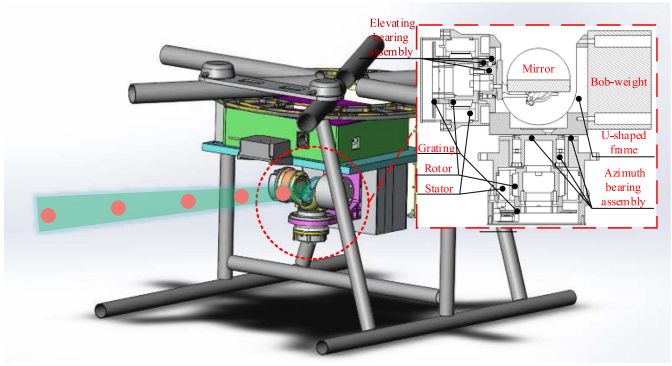

Fig. 3. Three-dimensional simple model of prototype. The two-axis mirror is installed below the prototype to suppress jitter, which adopts the integrated design. The mirror assembly and the driving grating assembly are symmetrically arranged. A counterweight is installed on the other side of the U-shaped frame, so that the azimuth axis can achieve the balance. Total weight is about 1.5 kg (counterweight is about 0.4 kg).

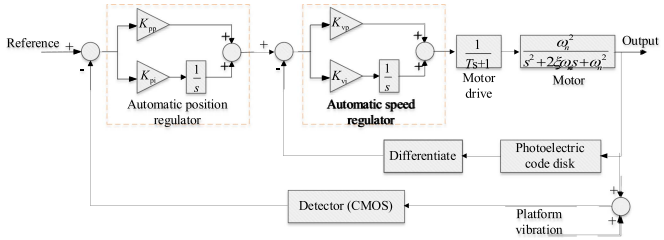

Fig. 4. Tracking system structure (in the APR, K_{pp} is the proportional gain and K_{pi} is the differential gain; in the ASR, K_{vp} is the proportional gain and K_{vi} is the differential gain; the motor drive circuit can be equivalent to a first-order inertial system; the detector can be regarded as a first-order delay system).

proportional integral differential (PID) control is no longer applicable. The reason is that the back electromotive force (EMF) in the current loop easily causes the system to oscillate, and the disturbance cannot be ignored. Here, dual-loop PI control is adopted. In the speed loop, the feedback is the motor speed, which is obtained by differentiating the absolute angle measured by the circular grating. and the sampling frequency is 2000 Hz; in the position loop, the feedback is provided by the centroid of the beacon light on the detector, and the sampling frequency is 200 Hz. The control system structure diagram is shown in Fig. 4. When the spot energy received by the detector is greater than the preset energy threshold, the centroid of the spot will be calculated, and the control board will use the difference between the actual centroid and the target centroid (reference input) as the input of the automatic position regulator (APR). Then, the speed command will be given passing through the APR, which is the input of the automatic speed regulator (ASR). Ideally, the error between the input and output of the control system is zero, but in practical systems, errors are unavoidable.

The components and control algorithms used in the azimuth motor and the pitch motor are identical, and the only difference is the motor load. Here, we take the azimuth motor as an example to illustrate the simulation results of the control system. Tracking errors are caused by residual loop error (noise equivalent angle) and uncorrected line-of-sight jitter, and obviously in simulation, the tracking errors are equivalent to residual line-of-sight jitter. The simulation system is built in Simulink. Fig. 5 shows the performance of the system against interfering signals. The system can suppress the noise signal in low-frequency band. The bode diagram of the tracking system is shown in Fig. 5(a), which shows that the system bandwidth is about 20 Hz. Fig. 5(b) shows the vibration data measured from the UAV platform and the tracking errors are obtained by inputting the vibration data into the control system as a disturbance signal. The errors are mainly limited to the range of ± 0.5 mrad. Fig. 5(c) shows power spectrum comparison of raw disturbance and residual line-of-sight jitter, which is consistent with Fig. 5(a).

IV. Acquisition Method

Acquisition is basic requirement in building the optical links. Scanning staring is generally used in optical quantum communications to capture beacons. However, due to the large uncertainty area of UAVs, the rapid establishment of drone-to-ground links cannot benefit from this method. Here, a new method for fast capture using GNSS information is implemented.

This algorithm involves the transformation between three coordinate systems: Earth-Centred, Earth-Fixed (ECEF), WGS-84 (World Geodetic System-1984), and North East Down (NED). For ECEF, the origin is the centre of mass of the earth, the X-axis points to the intersection of the prime meridian and the equator, and the Z-axis coincides with the rotation axis of the earth pointing to the north pole and forms a right-handed coordinate system with the Y-axis. WGS-84 is composed of longitude, latitude and altitude. In this article, the position information obtained by IMU is in this coordinate system. For NED, the origin is a certain point on the earth's surface, the X-axis points north, the Z-axis points down perpendicular to the earth's surface at this point, and the Y-axis points east according to the right-hand rule.

Suppose there is a point A on the earth, which is *(x, y, z)* in ECEF, *(b, l, h)* in WGS8, and *(n, e, d)* in NED; the following transformation relationships exist:

$$\begin{bmatrix} x \\ y \\ z \end{bmatrix} = \begin{bmatrix} (N+h)*\cos(b)*\cos(l) \\ (N+h)*\cos(b)*\sin(l) \\ \left(N*\left(1-\mathrm{e}^2\right)+h\right)*\sin(b) \end{bmatrix} \tag{2}$$

$$\begin{bmatrix} n \\ e \\ d \end{bmatrix} = \begin{bmatrix} -\sin(b)*\cos(l) & -\sin(b)*\sin(l) & \cos(b) \\ -\sin(l) & \cos(l) & 0 \\ -\cos(b)*\cos(l) & -\cos(b)*\sin(l) & -\sin(b) \end{bmatrix} * \begin{bmatrix} x \\ y \\ z \end{bmatrix} \tag{3}$$

where b is the latitude value, l is the longitude value, h is the height value, e^2 is the first eccentricity of the earth, N is the normal length, and $\mathrm{e}^2 = (\mathrm{a}^2 - \mathrm{b}^2)/\mathrm{a}^2$, $N = \mathrm{a}/\sqrt{1-\mathrm{e}^2*\sin^2(b)}$, $\mathrm{a} = 6378137$ meters, and $\mathrm{b} = 6356752.314$ metres.

In GNSS, the position of the ground station is (b_1, l_1, h_1), and that of the UAV is (b_2, l_2, h_2). According to (2), the position of the ground station is (x_1, y_1, z_1) and that of the UAV is

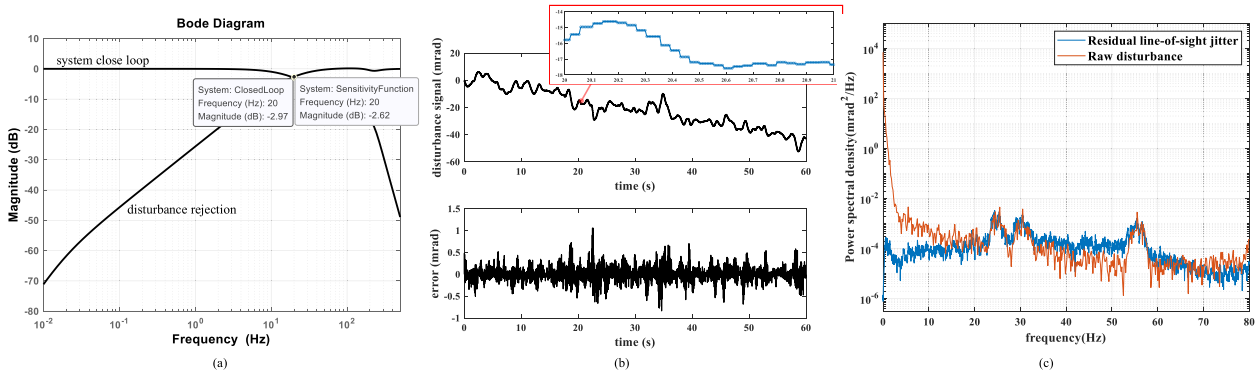

Fig. 5. (a) Bode diagram of system closed-loop transfer function and Bode diagram of error transfer function (sensitivity function). Bandwidth is up to about 20 Hz. (b) The first sub-plot is simulated disturbance signal. The disturbance signal is the yaw attitude angle of the UAV measured by IMU during the flight test of the UAV (The sampling frequency of IMU is 167 Hz, and due to limited by angular resolution, the same value appears continuously). It is taken as the disturbance input to obtain the output error data. Attached is a graph showing higher time resolution. The second sub-plot is simulated residual line-of-sight jitter. (c) Power spectrum comparison of raw disturbance and residual line-of-sight jitter. It shows that the system can significantly suppress the noise signal below 10 Hz.

(x_2, y_2, z_2) in ECEF. The UAV position is regarded as the base point to obtain the vector $\mathbf{V_{ECEF}} = (x_1 - x_2, y_1 - y_2, z_1 - z_2)$. Through the transformation of (3), $\mathbf{V_{NED}} = (v_n, v_e, v_d)$ is obtained. In flight, due to the change of the attitude, pointing exactly cannot be achieved only by $\mathbf{V_{NED}}$, and it is necessary to compensate for the attitude disturbance. Here, the rotation matrix, i.e., the Givens transformation, is introduced.

$$\begin{bmatrix} v_n' \\ v_e' \\ v_d' \end{bmatrix} = \mathbf{G}_1\mathbf{G}_2\mathbf{G}_3 \begin{bmatrix} v_n \\ v_e \\ v_d \end{bmatrix}$$

$$\mathbf{G}_1 = \begin{bmatrix} \cos(yaw) & \sin(yaw) & 0 \\ -\sin(yaw) & \cos(\text{yaw}) & 0 \\ 0 & 0 & 1 \end{bmatrix}$$

$$\mathbf{G}_2 = \begin{bmatrix} \cos(pitch) & 0 & -\sin(pitch) \\ 0 & 1 & 0 \\ \sin(pitch) & 0 & \cos(pitch) \end{bmatrix}$$

$$\mathbf{G}_3 = \begin{bmatrix} 1 & 0 & 0 \\ 0 & \cos(\text{roll}) & \sin(roll) \\ 0 & -\sin(roll) & \cos(roll) \end{bmatrix} \quad (4)$$

where *yaw* is around the Z axis (Down), *pitch* is around the Y axis (East), *roll* is around the X axis (North), and $\mathbf{V_{NED}'} = (v_n', v_e', v_d')$ is the new pointing vector.

In addition, if the direction of installing the IMU is inconsistent with that of the UAV, $\mathbf{V_{NED}'}$ needs to be rotated through the installation angle to obtain a new pointing vector $\mathbf{V_{NED}''} = (v_n'', v_e'', v_d'')$. Then, the azimuth and pitch angles of the two-axis mirror are calculated (5). After the two-axis mirror faces the ground station, the beacon from the ground can be captured.

$$\begin{bmatrix} Az \\ El \end{bmatrix} = \begin{bmatrix} \arctan\left(\frac{v_n''}{v_e''}\right) \\ -0.5{*}\arctan\left(v_d''/\sqrt{v_n''^2 + v_e''^2}\right) \end{bmatrix} \quad (5)$$

Fig. 6. (a) Airborne prototype (100 mm length for reference and the optical platform hole spacing: 25 mm). (b) 7 km air-to-ground link demonstration.

where Az is the azimuth and El is the elevation.

V. Experimental Verification

The acquisition and tracking system prototype is suspended below the UAV platform through WRI (Fig. 6(a)). Here is a brief introduction to WRI. WRI consists of a metal wire rope made up of individual wire strands that are in frictional contact with each other held between two parallel metal plates. For platform vibration, the WRI can provide flexibility in all directions and

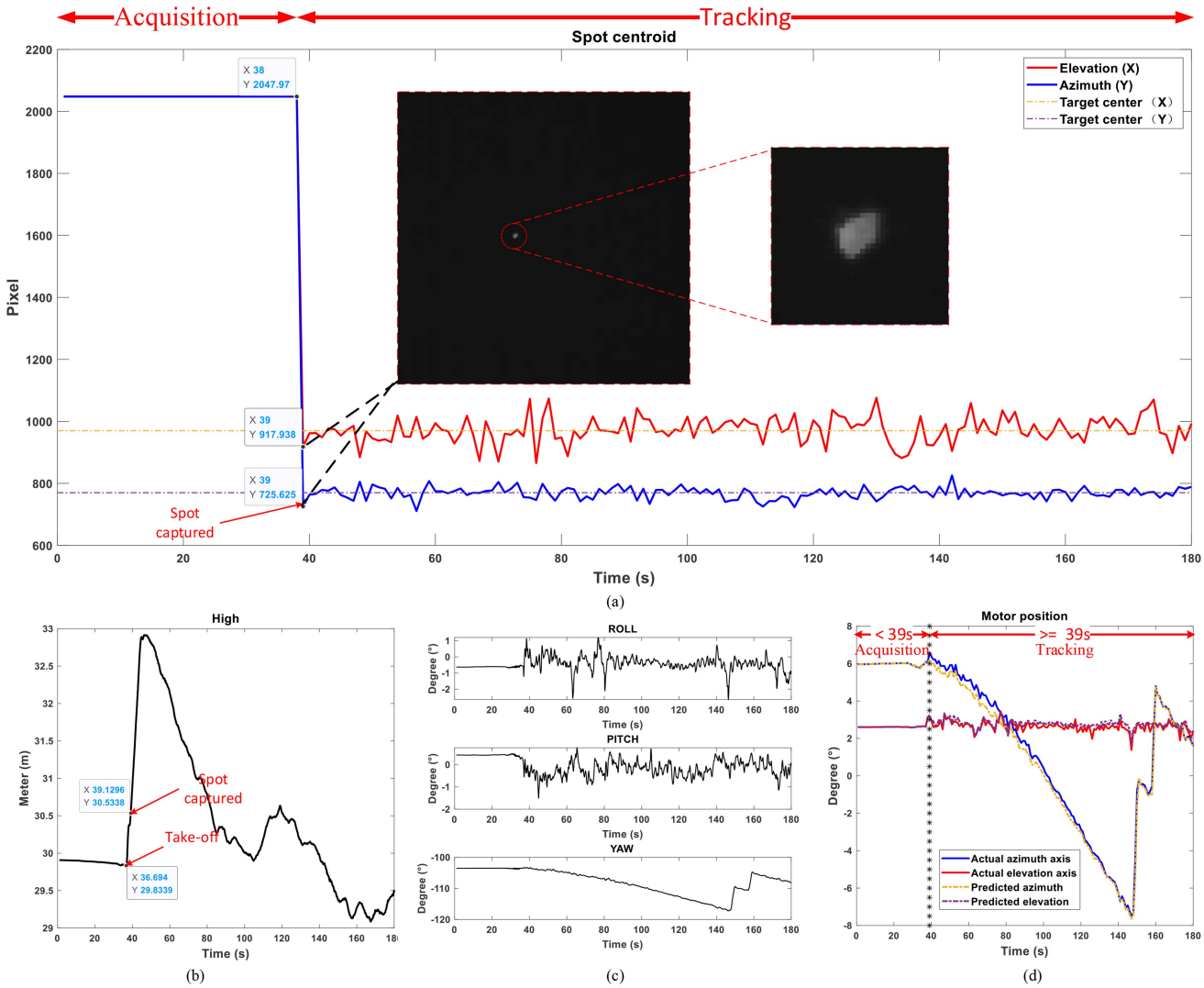

Fig. 7. Telemetry output. It describes the process of link establishment, the UAV from standstill to flight, and the system from acquisition to tracking (a) Spot centroid in the camera versus time. The centroid coordinate (2047.97, 2017.97), indicates that no spot is detected in the camera. The camera is in capture mode for the first 38 seconds, and the spot is captured at 39 seconds. Then the camera enters the tracking mode and jumps slightly near the target point (970770). Attached is the captured spot image. (b) UAV height path. The drone takes off at 36s, and it takes about 3 seconds from take-off to capture of the spot. (c) UAV attitude angle versus time. The main change is yaw in flight. (d) Actual pointing angle of the two-axis mirror and predicted pointing angle obtained by IMU. In the acquisition stage (<39s), the predicted angle determines the actual angle of the two-axis mirror; In the tracking stage, the output of the tracking control system determines the actual angle.

possesses inherent damping characteristics derived from rubbing and sliding friction between the intertwined cables absorbing vibration energy. Experiments show that the WRI can effectively overcome high-frequency vibrations, reducing the pressure of the tracking system. Moreover, the WRI is easily installed, light in weight, maintenance-free and low in cost, which is suitable for vibration isolation of small platforms. More descriptions about WRI can be found in references [24], [25].

The experimental site is located in Shanghai, China, a typical large city environment (Fig. 6(b)). During the experiment, in addition to the ATP system, the communication terminal is fixed under the UAV platform, which is close to the ATP system. For the communication terminal, the airborne system sends quantum light while the ground station receives these, and communication light is detected by four silicon avalanche photon diodes (APDs). The UAV takes off from the top of a building (5th-floor) at USTC Shanghai Institute for Advanced Studies (31°7′48″N, 121°33′6″E), while the ground station is placed near a window on the 16th-floor of a building at the YiCui Mansion (31°11′12″N, 121°31′8″E). The ground terminal pointed the 671-nm uplink beacon laser at the drone in advance. Fig. 7 describes the whole process of link establish-ment. After the system starting, it automatically enters the acquisition mode and generates a predicted pointing according to the position and attitude of the UAV. The predicted angle determines the actual angle of the two-axis mirror in the acquisition stage (Fig. 7(d)) At the initial moment, the UAV is still on the ground, and the link could not be established due to the obstruction of surrounding buildings. Before 36s, the UAV is stationary (no change in attitude). At 36s, the UAV takes off (Fig. 7(b)) and the platform

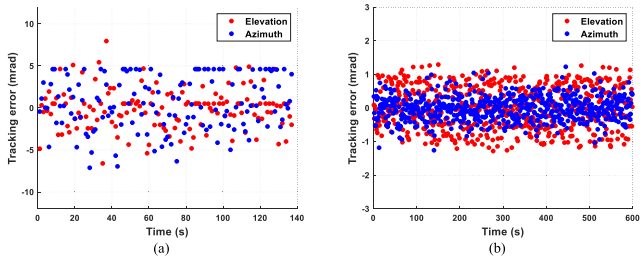

Fig. 8. (a) Tracking errors without isolation. (b) Tracking errors after isolation.

begins to vibrate (Fig. 7(c)). The camera then captured the light spot at 39s (Fig. 7(a)). The ground station is not in the FOV of the camera until the UAV is at a certain height, which results in a difference of about 3 seconds. At the same time, the ground station also captures the beacon from the airborne system, and the link is successfully established. After the acquisition having implemented, the tracking mode is entered. At the later time, the UAV is moved through the air to test the tracking performance of the system. The system can continuously track the beacon from the ground station, and the spot in the camera jumps slightly at the target position (Fig. 7(a)). In the tracking stage, the output of the tracking control system determines the actual angle, while predicted pointing does not work (Fig. 7(d)). It is worth mentioning that even in the tracking stage, the difference between the predicted angle and the actual angle is small, and the main source of the difference is that the attitude and position information provided by the IMU is not accurate enough. The attitude of the UAV determines the pointing angle of the two-axis mirror, which is particularly evident in the correlation between the yaw angle of the UAV and the azimuth axis angle of the tracking system. Due to the violent movement of the UAV platform or atmospheric turbulence, there is a possibility of losing the detected beacon in the camera. In this case, the ATP system can restart the acquisition and continue the experiment automatically.

To demonstrate the utility of WRI, two tests are conducted, one without WRI and the other with WRI. The performance of the acquisition and tracking system without isolation is tested first, and a section of tracking error data is intercepted. Here, the difference between the spot centroid and the target point is converted into milliradians. Fig. 8(a) shows that the tracking errors have reached $\pm$ 5 mrad. Obviously, the quantum communication link cannot be built at all in this state. Nevertheless, the experimental results show that when the beacon jumps out of the FOV, the system can quickly reacquire the beacon, which verifies the rapidity of acquisition. Then, the prototype was connected to the drone platform via the WIR. Fig. 8(b) shows the tracking errors lasting 10 minutes. The errors are basically within 1 milliradian. The standard deviation of the azimuth direction error is $358\ \mu\mathrm{rad}$, and that of the pitch direction error is $617\ \mu\mathrm{rad}$. Compared with the experimental results without the isolation device, the tracking accuracy is significantly improved, which verifies the feasibility of the tracking system. However, the pitch direction performance is slightly worse. It is believed that the error can be reduced by optimizing the control algorithm or optimizing the isolation device in the future.

VI. Conclusion

In this article, a SWaP acquisition and tracking prototype is designed to build airborne QKD link, which can quickly acquire and stably track the beacon light from long-distance ground stations. The system adopts the transceiver coaxial structure, featuring a compact footprint and easy integration with existing modules. In performance, the large FOV of the camera and the fast motor response enable long-distance link establishment. Moreover, a special isolation unit is used: the WRI, which is lightweight and suitable for small platforms. In the 7 km air-to-ground demonstration, a small six-rotor UAV was used as a platform to test the prototype. The link remained stable for up to 10 minutes, proving that the system has the ability to quickly and automatically align.

The focus of this work is not on a particular subsystem. In fact, individual subsystems or components can be further studied and discussed or improved by better engineering. For example, higher integration can make the system more compact, and the isolation system can be further optimized to adapt the ATP system. Under the existing hardware, using the attitude angle provided by IMU for feed forwards augment PID control can improve the system bandwidth. Furthermore, the SWaP acquisition and tracking system can not only support QKD link, but also support general long-range FSO link, which provides an approach to the design of small acquisition and tracking systems and serves airborne optical quantum deployment in real environments.

References

[1] A. Singh, K. Dev, H. Siljak, H. D. Joshi, and M. Magarini, "Quantum internet-applications, functionalities, enabling technologies, challenges, and research directions," *IEEE Commun. Surv. Tut.,* vol. 23, no. 4, pp. 2218–2247, Oct.–Dec. 2021.

[2] S. H. Wei et al., "Towards real-world quantum networks: A review," *Laser Photon. Rev.,* vol. 16, Jan. 2022, Art. no. 2100219.

[3] H. L. Yin et al., "Measurement-device-independent quantum key distribution over a 404 km optical fiber," *Phys. Rev. Lett.,* vol. 117, no. 19, Nov. 2016, Art. no. 190501.

[4] S. Wengerowsky, S. K. Joshi, F. Steinlechner, H. Hubel, and R. Ursin, "An entanglement-based wavelength-multiplexed quantum communication network," *Nature,* vol. 564, no. 7735, pp. 225–228, Dec. 2018.

[5] S. K. Liao et al., "Satellite-to-ground quantum key distribution," *Nature,* vol. 549, no. 7670, pp. 43–47, Sep. 2017.

[6] H. Takenaka, A. Carrasco-Casado, M. Fujiwara, M. Kitamura, M. Sasaki, and M. Toyoshima, "Satellite-to-ground quantum-limited communication using a 50-kg-class microsatellite," *Nature Photon.,* vol. 11, no. 8, pp. 502–508, Aug. 2017.

[7] H. Y. Liu et al., "Drone-based entanglement distribution towards mobile quantum networks," *Nat. Sci. Rev.,* vol. 7, no. 5, pp. 921–928, May 2020.

[8] A. Kumar et al., "Survey of promising technologies for quantum drones and networks," *IEEE Access,* vol. 9, pp. 125868–125911, 2021.

[9] Y. Xue, W. Chen, S. Wang, Z. Q. Yin, L. Shi, and Z. F. Han, "Airborne quantum key distribution: A review [Invited]," *Chin. Opt. Lett.,* vol. 19, no. 12, Dec. 2021, Art. no. 122702.

[10] Optics.org, "50Mbit/s laser link between aircraft and satellite," Dec. 22, 2006. [Online]. Available: https://optics.org/article/26701

[11] Z. Q. Xu, "Application research of tethered UAV platform in marine emergency communication network," *J. Web Eng.,* vol. 20, no. 2, pp. 491–511, 2021.

[12] R. Sahoo and P. Shanmugam, "Effect of the complex air–sea interface on a hybrid atmosphere-underwater optical wireless communications system," *Opt. Commun.,* vol. 510, 2022, Art. no. 127941.

[13] L. B. Kumar and P. Krishnan, "Multi-hop convergent FSO-UWOC system to establish a reliable communication link between the islands," *Opt. Commun.,* vol. 474, 2020, Art. no. 126107.

[14] H. S. Khallaf and M. Uysal, "Comprehensive study on UAV-based FSO links for high-speed train backhauling," *Appl. Opt.,* vol. 60, no. 27, pp. 8239–8247, Sep. 2021.

[15] A. V. Vo, D. F. Laefer, and M. Bertolotto, "Airborne laser scanning data storage and indexing: State-of-the-art review," *Int. J. Remote Sens.,* vol. 37, no. 24, pp. 6187–6204, 2016.

[16] Q. Li, L. Liu, X. F. Ma, S. L. Chen, H. Yun, and S. Tang, "Development of multitarget acquisition, pointing, and tracking system for airborne laser communication," *IEEE Trans. Ind. Inform.,* vol. 15, no. 3, pp. 1720–1729, Mar. 2019.

[17] A. B. Raj and A. K. Majumder, "Historical perspective of free space optical communications: From the early dates to today's developments," *IET Commun.,* vol. 13, no. 16, pp. 2405–2419, Oct. 2019.

[18] R. J. Feldmann and R. A. Gill, "Development of laser crosslink for airborne operations," in *Proc. IEEE Mil. Commun. Conf.*, 1998, pp. 633–637.

[19] R. Arnold et al., *500-km 1-GBPS Airborne Laser Link (Optoelectronics and High-Power Lasers and Applications)*. Bellingham, WA, USA: SPIE, 1998.

[20] W. Griethe, M. Gregory, F. Heine, and H. Kampfner, "High speed laser communications in UAV scenarios," in *Airborne Intelligence, Surveillance, Reconnaissance (ISR) Systems and Applications VIII*. Bellingham, WA, USA: SPIE, 2011.

[21] H. Haan and C. Siemens, "Airborne optical communication terminal: First successful link from tenerife to the GEO alphasat," in *Laser Communication and Propagation through the Atmosphere and Oceans VIII*. Bellingham, WA, USA: SPIE, 2019.

[22] X. M. Li, L. Z. Zhang, and L. X. Meng, "Airborne space laser communication system and experiments," *Proc. SPIE,* 2015, pp. 98–108.

[23] F. Moll et al., "Demonstration of high-rate laser communications from a fast airborne platform," *IEEE J. Sel. Areas Commun.,* vol. 33, no. 9, pp. 1985–1995, Sep. 2015.

[24] S. Rashidi and S. Ziaei-Rad, "Experimental and numerical vibration analysis of wire rope isolators under quasi-static and dynamic loadings," *Eng. Structures,* vol. 148, pp. 328–339, Oct. 2017.

[25] P. S. Balaji, M. E. Rahman, L. Moussa, and H. H. Lau, "Wire rope isolators for vibration isolation of equipment and structures - A review," in *Proc. 9th Curtin Univ. Technol. Sci. Eng. Int. Conf.,* 2015, Art. no. 012001.